Microscopic collective dynamics in liquid *para*-H_2

F. J. Bermejo
Instituto de Estructura de la Materia, CSIC, Serrano 123, E-28006 Madrid, Spain

B. Fåk
Commissariat à l'Energie Atomique, Département de Recherche Fondamentale sur la Matière Condensée, SPSMS/MDN, 38054 Grenoble, France

S. M. Bennington
Rutherford Appleton Laboratory, Chilton, Didcot, Oxon OX11 OQX, United Kingdom

R. Fernández-Perea
Argonne National Laboratory, Argonne, Illinois 60439

C. Cabrillo
Instituto de Óptica, CSIC, Serrano 121, E-28006 Madrid, Spain

J. Dawidowski
Centro Atómico Bariloche, 8400 San Carlos de Bariloche, Rio Negro, Argentina

M. T. Fernández-Diaz
Institut Laue Langevin, Boîte Postale 156, F-38042 Grenoble Cedex 9, France

P. Verkerk
Interfaculty Reactor Institute, Mekelweg 15, 2629 JB Delft, The Netherlands

(Received 27 May 1999)

Well-defined phonons with strong anomalous (upward) dispersion are observed by inelastic neutron scattering in liquid *para*-H_2 at a temperature of 15.7 K. The damping, being very small for the low-Q phonons, increases with wave vector Q, and only broad features are observed for $Q \gtrsim 1$ Å^{-1}. This behavior is shown to deviate strongly from results of molecular simulations of a fully classical analogue using a realistic potential. [S0163-1829(99)01245-X]

I. INTRODUCTION

Hydrogen, which was first condensed by Dewar a century ago (1899) reaching a temperature of 12 K, continues to be a source of exciting new science. The interest in pursuing studies on this system stems from a variety of circumstances. First, it constitutes the most abundant element in the Universe, where it is found to appear in various states of aggregation stretching over a vast range of densities and temperatures, and it is known to be one of the dominant constituents of the giant planets such as Jupiter or Saturn.[1] Second, it is the simplest system of two distinguishable particles which allows a rigorous first-principles calculation and, furthermore, the problem of the interaction of two hydrogen molecules has been solved in a virtually exact manner. Finally, studies on fluid and/or condensed states of H_2 and its mixtures with elements such as He are of considerable interest, since such systems provide benchmarks for models of phase equilibria in mixtures under extreme conditions.

The peculiarities of the behavior of hydrogen in its fluid or solid phases can be tracked down to microscopic scales, where one finds that the intermolecular repulsion between a pair of H_2 molecules is considerably softer than that found for many other elements.[2] In addition, at temperatures below that where the gas condenses into a liquid ($\approx$20.4 K) under its saturated vapor pressure, the quantum nature of its atomic motions unveils itself by the appearance of a discrete spectrum of transitions between molecular rotational levels. This means that the rotational states and the nuclear-spin states of the two protons forming the H_2 molecule will not be independent. Two different species exist depending on the nuclear-spin degeneracy: *para*-H_2 (p-H_2) with a total nuclear spin $I=0$ and *ortho*-H_2 (o-H_2) with $I=1$. This fact adds very special characteristics to the interaction potential. Because of symmetry constraints imposed on the total molecular wave function, p-H_2 is in a spherically symmetric (s-wave-like) state and therefore particles within the ground state can be regarded as interacting through an isotropic potential, whereas o-H_2 (p-wave-like) will show a strong angular dependence in its interactions with neighboring particles due to the action of a finite electric quadrupole moment.

A further decrease of the temperature leads to freezing, $T_m \approx 14.5$ K, into a crystalline state where in addition to virtually free particle rotations one finds a solid where the lattice energy contains kinetic and potential contributions with

comparable weights. In other words, quantum zero-point vibrations take such a large amplitude ($\approx$18 percent of the distance between neighbors), that the description of the crystal in terms of a lattice formed by particles oscillating about well defined sites ceases to be valid. Such a crystal exhibits a number of remarkable anomalies in its transport properties. In particular, heat conduction in nearly pure p-H_2 is strongly anisotropic, a characteristic only expected for layered crystals such as graphite.[3] The phenomenon can be explained in terms of phonon-scattering mechanisms within the first Brillouin zone.[3] In other words, the understanding of a macroscopic property such as heat conduction requires the knowledge of the excitation spectra of the crystal on microscopic scales.

Here, we have set out to explore the dynamic response of liquid p-H_2 at scales of the order of an ansgtrom and a picosecond by measurement of the quantity $S(Q,\omega)$ accessible to both neutron scattering and computer simulations. For a liquid such as this, the total dynamic structure factor $S(Q,\omega)$, apart from peaks corresponding to single-particle excitations such as those arising from the recoiling particle after neutron impact and the $para \rightarrow ortho$ transitions with frequencies $\omega_{JJ}=7.35\ J(J+1)$ meV, where the coefficient stands for the rotational constant, is expected to show some finite-frequency peaks arising from the collective motions that should merge with those characteristic of hydrodynamic long-wavelength phonons at small values of the momentum transfer Q. The frequency of such peaks is thus expected to provide some information on the propagation of collective excitations at microscopic scales, and their linewidth will contain details about their lifetimes. Within the microscopic realm, both parameters are strongly dependent on the shape and strength of the interparticle potential, at least for fully classical bodies.[4] This is because the peak frequencies are governed by the elastic constant and the density of the medium, whereas the peak width arises from all those processes involved in the decay of an excitation such as heat conduction or viscous flow, and all these are found to be related to the interparticle potential.[5]

The rationale behind the present effort stems from the extreme sensitivity of the dynamics encompassed by $S(Q,\omega)$ in the molten state to fine details of the interaction potential. The expectation is that such a comparison will serve to gauge the state of our current knowledge of microscopic interactions in these exceedingly interesting substances on a more quantitative ground. In addition, we also sought to explain the origin of the rather high values for the thermal conductivity of liquid hydrogen, which is known to deviate largely from that of other liquified noble gases and heavy diatomics if scaled under ''corresponding states'' arguments.[6]

We have carried out a series of neutron-scattering experiments on (*mostly*) p-H_2, and compared the measured results for the most relevant spectral parameters defining a collective excitation (or a phonon in a crystalline solid) with those derived from computer calculation of a liquid sample composed of particles which interact through the Silvera-Goldman potential,[2] which is known to provide a realistic representation of interactions up to fairly high densities.[1] The comparison, which is carried out on almost classical grounds (the particles are taken as spherical and the interactions follow Newton laws), is supplemented with an additional confrontation with a full finite-temperature quantum treatment on the basis of the correlated density matrix theory (CDM).[7]

Although the results of neutron-scattering experiments on the collective excitations in liquid p-H_2 have been reported twice in the literature,[8,9] the difficulties inherent to such measurements (i.e., the need to catalyze the sample into a p-H_2 state, effective suppression of monochromator and analyzer higher harmonics, etc.) cast serious doubts on the soundness of the results reported from both experiments. In particular, the spectral intensities reported in Ref. 9 are dominated by harmonics of the $J\ 0\rightarrow 1$ rotational transition, leaving only a broad signal underneath as assignable to the sought excitation whose frequency cannot be estimated reliably. On the other hand, the data from Carneiro *et al.*[8] seem to be affected by the procedure employed to deconvolute the experimental intensities from resolution effects. This leads to the appearance of an extremely narrow peak at $Q=0.7$ Å^{-1} which is not readily seen in the raw intensities. Furthermore, both referred studies[8,9] were carried under rather restricted kinematic conditions which hinder the measurement up to the required energy transfers for momentum transfers below $\approx$0.8 Å^{-1}. Finally, apart from being mutually incompatible, both experiments are also at odds with results derived for liquid $ortho$-D_2,[10] with differences far larger than those attributable to the isotope and temperature effects, as well as with results from depolarized Raman measurements.[11] The latter show a broad, nonexponential spectrum with a flat maximum at about 8 meV and a width of approximately 9 meV. In stark contrast, the reported neutron results show either an extremely narrow (resolution limited) peak at large Q values,[8] or depict the characteristic frequencies of the excitations[9] on a scale well below those corresponding to Raman measurements as well as those of liquid o-D_2.

II. EXPERIMENT AND COMPUTER SIMULATION DETAILS

The neutron measurements were carried out using the MARI chopper spectrometer of the ISIS source at RAL as well as the IN8 thermal three-axis spectrometer at ILL (Grenoble). Choosing two rather different techniques was dictated by the difficulties alluded to in previous paragraphs which advised us to carry two independent measurements in order to prove the consistency of the measured data. The sample consisted of high-purity hydrogen gas, which was converted to p-H_2 by forcing it to pass through a bed of activated catalyst at low temperatures. Ni-supported silica was used on MARI and $Fe(OH)_3$ on IN8. The best results for the conversion were obtained by either condensing the sample very slowly ($\sim$6 h), or by letting the gas pass through the catalyst several times by boiling and recondensing it. Measurements of the static structure factor $S(Q)$ were used to determine the remaining amount of o-H_2, which gives a strong contribution to $S(Q)$ for $Q\rightarrow 0$. Several different spectrometer settings were employed to cover adequately the whole $Q-\omega$ space under optimum conditions. Relatively large incident energies, $E_i=40$ (34.8) meV on MARI (IN8), were used to cover sufficiently high-energy transfers at low Q's, with an energy resolution of 1.0 (2.7) meV on MARI (IN8). The region close to the peak in the

static structure factor $Q_p \approx 2$ Å^{-1} was explored with an improved energy resolution of 0.5 (0.8) meV on MARI (IN8) using $E_i \approx 15$ meV.

Because of the strong dependence of the scattering cross section with the energy of the incident neutrons,[12] measurements carried out on IN8 were performed on constant incident wave vector mode. This enables a direct comparison of data measured on the two instruments. Under the present experimental conditions, the amount of *para*-H_2 after catalysis remains in a steady state for a few days under neutron irradiation even if some of the incident neutrons are able to rotationally excite a small fraction of molecules into the *ortho* state [i.e., by an amount commensurable with the flux of neutrons going through the sample which is of the order of 10^7 neutrons cm^2 s^{-1} (IN8) and 10^4 neutrons cm^2 s^{-1} (MARI)].

Several calculations were carried out to estimate the contribution of multiply scattered neutrons to the measured spectra. The procedure followed to calculate such an effect was that reported in Ref. 13 which allows us to perform multiple-scattering and multiexcitation corrections. The estimate of multiply scattered neutrons was about six percent, an amount which was easily accounted for.

Constant-angle spectra as measured at MARI were processed using the instrument suite of programs which allows interpolation of the $S(\theta,\omega)$ surface into individual spectra for constant momentum transfer or constant energy transfer.

A number of computer simulations for a system mimicking liquid *p*-H_2 were also performed. The calculations were carried out at constant particle number, volume, and temperature (NVT algorithm) using the Silvera-Goldman potential.[2] It significantly differs from the standard Lennard-Jones form, and it reads

$$V(R) = \exp(\alpha - \beta r - \gamma r^2) + f(R)\left\{ \sum_{i=6,8,10} C_i / R^i + C_9 / R^9 \right\} \tag{1}$$

with

$$f(R) = \begin{cases} \exp\left\{ -\left[\left(1.28 \dfrac{R_m}{R} \right) - 1 \right]^2 \right\} & R < 1.28 R_m \\ 1 & R > 1.28 R_m \end{cases}, \tag{2}$$

where $\alpha = 1.713$, $\beta = 1.5671$, $\gamma = 0.00993$, $C_6 = -12.14$, $C_8 = -215.2$, $c_10 = -4813.9$, and $C_9 = 143.1$, all in atomic units, and $R_m = 3.41$ Å.

The simulations were carried out on a system of 613 particles within a box of 29.96 Å of side which result in a density of 0.0763 g/cm^3. The calculated trajectories span 0.125 ns, which results in a resolution in frequency space for the calculated dynamic structure factor $S_{sim}(Q,\omega)$ of 0.02 meV.

III. RESULTS

An overview of the spectra measured with the MARI spectrometer is provided by the contour plots shown in Fig. 1. Apart from the strong intensity arising from the peak in $S(Q)$ at $Q_p \approx 2$ Å^{-1} and the rotational line at $\omega \approx 14.5$ meV, there is a dispersive (Q-dependent) feature that is clearly seen as a color stripe. It extrapolates to zero energy for $Q \to 0$, passes through a maximum at $Q_p/2 \approx 1$ Å^{-1} and decreases in frequency from here down to Q_p, where it approaches a clear minimum. Such wave vector dependence of the inelastic intensities rules out the presence within our measured data of any large contribution arising from particle recoil scattering effects. A recoil scattering signal attributable to the $J\ 0 \to 0$ transition is expected to appear as a peak whose frequency varies as $\hbar^2 Q^2 / 2M_H$, its intrinsic width is linear in Q and its amplitude becomes maximal as $Q \to 0$. From the extensive recoil scattering data reported by Langel *et al.*[14] the effective mass is known to be very close to the molecular mass $M_H = 2$ amu so that the recoil signal would appear at ≈ 1.04 meV for $Q = 1$ Å^{-1} and ≈ 4.2 meV for $Q = 2$ Å^{-1}, that is well separated from the strong, dispersive signal. In addition, the recoil line is expected to be rather weak within the range of explored momentum and energy transfers in the light of results from recoil scattering experiments such as those reported by Langel *et al.*[14]

A set of individual $I(Q,\omega)$ spectra as measured by both instruments is shown in Fig. 2 and Fig. 3. The left-hand side of Fig. 2 depicting data measured at IN8 reveals that a well defined (i.e., nonoverdamped) excitation is supported by the fluid, at least for wave vectors below 0.8 Å^{-1}. Above such a value the broadening becomes comparable to the peak frequency indicating that excitations have decayed considerably at such length scales. A broad peak is still visible at wave vectors well beyond $Q_p/2$, where $Q_p \approx 2$ Å^{-1} stands for the maximum of the static structure factor, a quantity which is also depicted in the right-hand side of the referred figure. Notice that at low wave vectors, $Q \leqslant 0.4$ Å^{-1}, the linewidth of the excitation becomes remarkably small (well below the resolution), which clearly indicates that the excitation mean-free path becomes comparable or larger than the characteristic distance $d = 2\pi/Q$. For Q values above $Q_p/2$, an inelastic peak is still seen at frequencies between those comprising the elastic peak and the $J = 0 \to J = 1$ rotational transition. However, their characteristic widths are so large, $\Gamma_Q \simeq \Omega_Q$, that these excitations are to be considered as very heavily damped. Finally, a strong softening occurs, as expected, for wave vectors near Q_p, as shown in the lower right-hand side of Fig. 2.

To enable a direct comparison of the raw data, Fig. 3 displays a set of constant-Q and constant-ω spectra as measured using the MARI spectrometer. As can easily be seen from an inspection of the left-hand side part of Fig. 3, the same features are here observed, the main differences being entirely attributable to different resolution functions, counting statistics, and signal/background ratios. To ascertain the acoustic character of the excitation being sampled, the right-hand side of Fig. 3 depicts the static structure factor $S(Q)$ (integrated over the explored range of energy transfers) as well as a set of $I(Q, \omega = const.)$ constant energy-transfer sections of the $Q-\omega$ surface. The $S(Q)$ structure factor again shows its main peak at $Q_p \approx 2$ Å^{-1} as well as a second maximum at about 3.5 Å^{-1}. The absence of any sizeable incoherent scattering in the graph just referred to [i.e., the peaks in $S(Q)$ would appear superposed to a strong Q-dependent ''droop'' otherwise] ensures that most of the sample is in *para* state and this also sets limits to the contribution of single particle (i.e. recoil scattering) which, al-

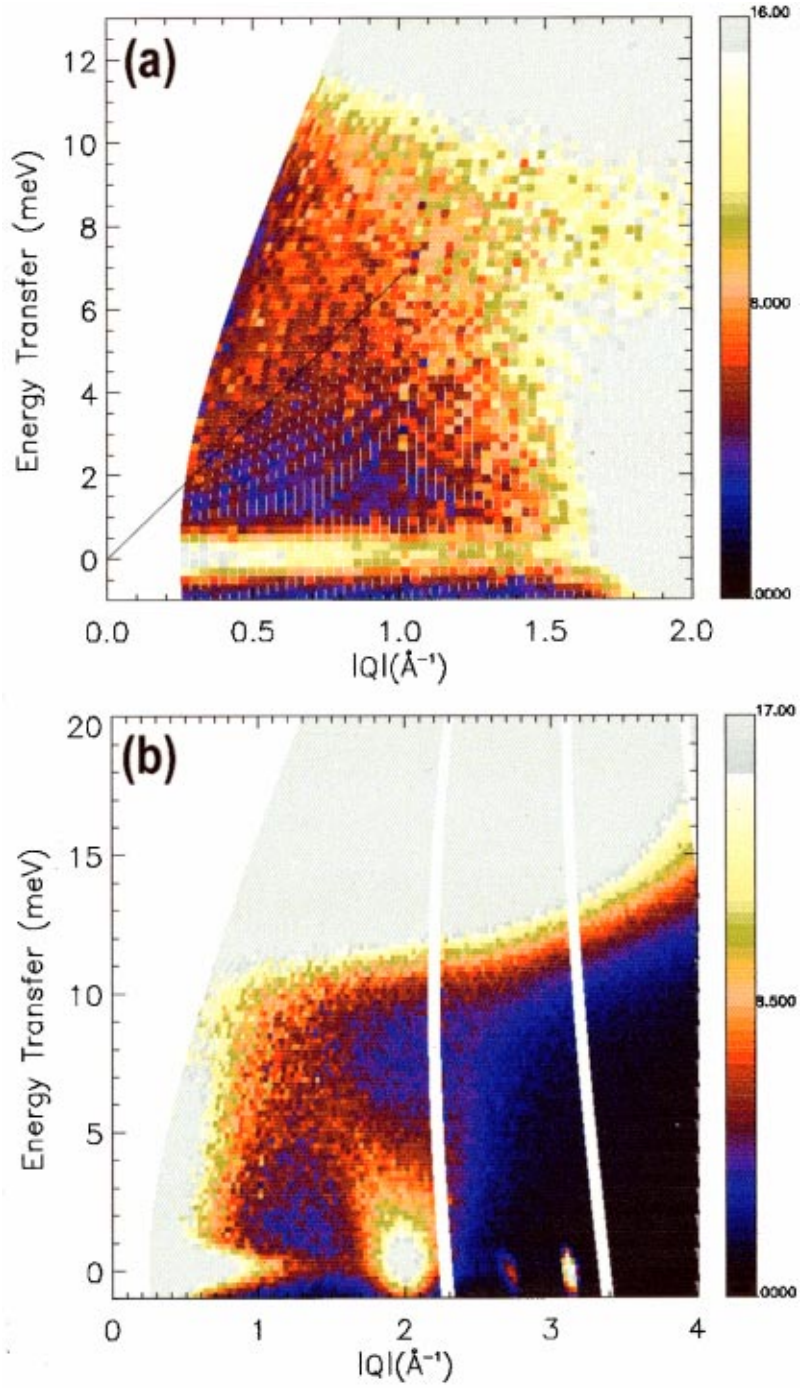

FIG. 1. (Color) Contour plots of the measured $I(Q,\omega)$ of liquid *para*-H_2 at $T=15.7$ K. (a) Surface depicting the lower-Q region. Notice the dispersion of collective excitations which appears as a red stripe of increasing width reaching a maximum of ≈ 8 meV. The strong intensity about $Q=2$ Å^{-1} arises from the peak in the static structure factor, while that above 12 meV comes from the neutron induced $para \rightarrow ortho$ transitions. (b) The spectra are here divided by Q^2 (a trivial factor governing the inelastic intensity of a condensed body) to facilitate visualization. Notice the red stripe signaling the dispersion coming down from a maximum of ≈ 8 meV at $Q \approx 1$ Å^{-1}.

though has to be present in all the range of explored wave vectors, shows here a strength much too small if compared with that of the coherent response.

For an excitation of purely acoustic nature one expects that all the characteristic equilibrium distances of the liquid are not altered, since the motion mainly involves in-phase displacements of its constituting particles. This is indeed what is seen. A clear peak at $Q=Q_p$ appears in the referred quantities up to frequencies of 8 meV, and the same applies to the subsidiary maximum at 3.5 Å^{-1}. The graph on the bottom-right corner of Fig. 3 depicts an equivalent quantity for an energy transfer which nearly matches the frequency of the neutron-induced $para \rightarrow ortho$ rotational transition. As can be seen, no trace of the peaks at 2 Å^{-1} and 3.5 Å^{-1} is seen there. The intensity of such a curve follows[15]

$$I(Q,\omega=14.5 \text{ meV}) \propto \exp(-Q^2\langle u^2\rangle/3) j_1^2(Qr_{HH}), \quad (3)$$

where the exponential stands for a Debye-Waller term with includes a mean-square displacement $\langle u^2\rangle$ of the molecules, j_1 is a spherical Bessel function, and r_{HH} is the internuclear equilibrium separation between the two protons forming a molecule. A fit of Eq. (3) to the data shown in Fig. 3 yields a value for the mean-square displacement of $\langle u^2\rangle = 0.95 \pm 0.2$ Å^2, which is to be compared with that of 0.48 Å^2 derived for the crystal at 5.4 K using the same procedure. The figure found for the liquid may be compared with the value of 0.36 Å^2 computed from $\langle u^2\rangle = 6D\tau_0$ where D stands for the measured translational self-difussion coefficient[16] which amounts to 0.47 Å^2 ps^{-1} and τ_0 for the inverse of the observation frequency. The comparison thus

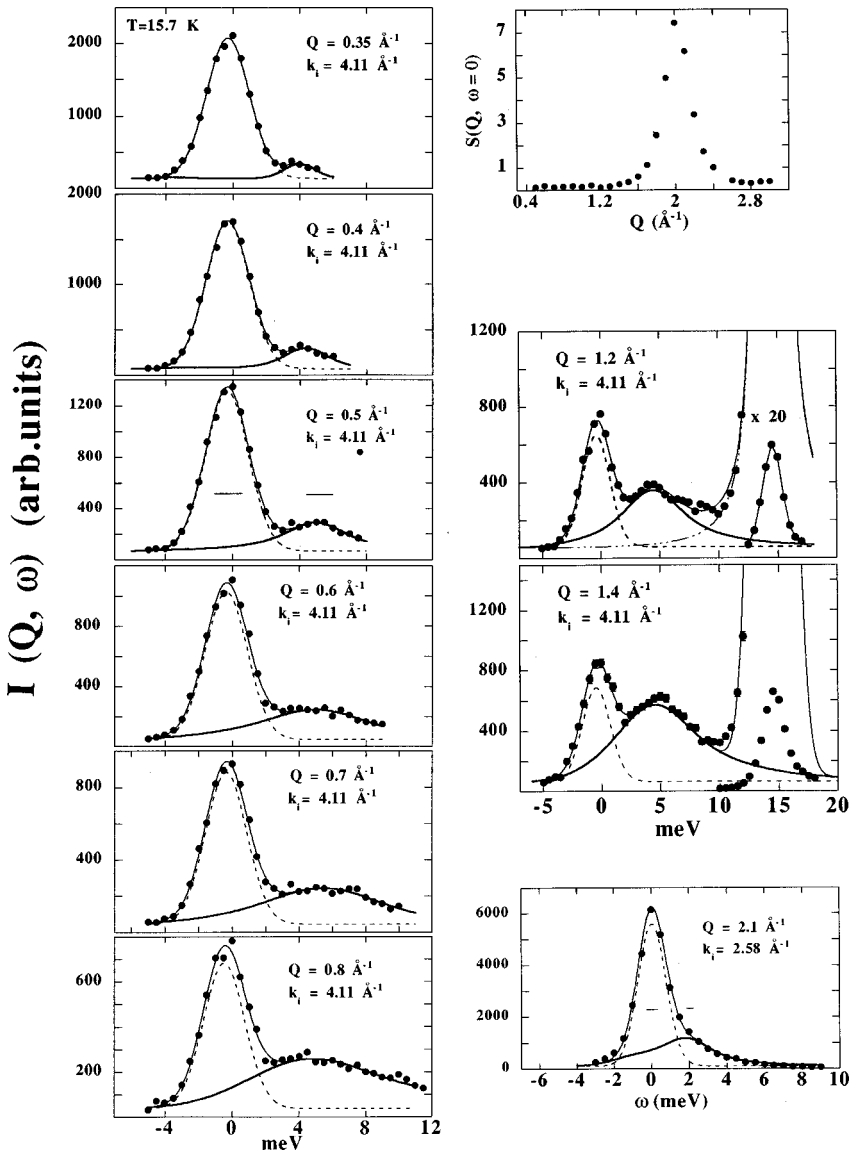

FIG. 2. The left-hand side depicts constant-Q spectra for wave vectors below $Q_p/2$ as measured using the IN8 spectrometer. The Q values as well as the incident wave vector are given as insets. Filled circles with error bars represent the measured data. The thin solid line shows the model fit (see text), the dashed line the fitted $I_{qel}(Q,\omega)$ intensity, and the thick solid line depicts the inelastic contribution $I_{inel}(Q,\omega)$ to the total intensity. The upper right-hand-side frame shows the quantity $S(Q,\omega=0)$ that is the zero-energy transfer integrated over the resolution volume. It represents the quantity continuously monitored to check whether significant amounts of *ortho*-H_2 were present within the sample. Its large cross section gives rise to a huge incoherent-scattering contribution easily detectable as a strong riseup of intensity as $Q \rightarrow 0$. The rest of the graphs in the right-hand side of the figure depict spectra corresponding to wave vectors close to $Q_p/2$ (1.2 Å^{-1}), at Q_p (2.1 Å^{-1}) and somewhere between those (1.4 Å^{-1}). Notice the strong peak arising from the $J=0\rightarrow J=1$ transition centered close to 15 meV.

shows that a large portion of the measured displacement cannot be assigned to difussive, single-particle motions. Instead, zero-point atomic vibrations appear as the most sensible candidates to explain the missing amplitude.

To describe the measured intensities in terms of physical parameters, a model scattering law was convoluted with the wave vector and frequency-dependent instrumental resolution function $R(Q,\omega)$ and fitted to the observed spectra. The simplest model able to reproduce the observations is given in terms of a damped harmonic oscillator (DHO) plus a quasielastic contribution which is introduced to reproduce the shape of the central peak. Choosing the functional form of a DHO to represent the inelastic intensities is here fully justified since, as in the case of liquid He,[17] one only has to account for the excitations corresponding to a fluid composed by particles which are identical and effectively spherical.

The model scattering law thus reads,

$$I_{mod}(Q,\omega)=[n_B(\omega)+1][I_{qel}(Q,\omega)+I_{inel}(Q,\omega)+I_{rot}(Q,\omega)]\otimes R(Q,\omega)+B, \quad (4)$$

where $n_B(\omega)$ is the Bose function, B a constant background term, and $I_{qel}(Q,\omega)$ is the central peak, which includes both the quasielastic response from the liquid as well as elastic scattering from the Al container. The contribution from rotational $J=0\rightarrow J=1$ transitions, $I_{rot}(Q,\omega)$, needs to be included for spectra measured for $Q=Q_p/2$ and beyond. It was modeled as a Gaussian centered at $E_{10}=\omega_{10}+E_R$, where the second term stands for the recoil energy of a hydrogen molecule of mass M_H which was referred to above.

The inelastic neutron-scattering response of a liquid composed by effectively spherical particles interacting through a central potential will only show one mode which corresponds to collective longitudinal density fluctuations. The explicit form used to model the spectrum shape $I_{inel}(Q,\omega)$ using the damped harmonic oscillator function was taken from Ref. 17 and reads $Z_Q 2\omega\omega_Q\Gamma_Q[(\omega^2-\Omega_Q^2)^2+4\omega^2\Gamma_Q^2]^{-1}$, where $\Omega_Q^2=\omega_Q^2+\Gamma_Q^2$.

The quality of the fits can be gauged from Figs. 2 and 4. No significant information could be derived from the central component, since the energy resolution was too large compared with the quasielastic linewidths. As can be seen from the shown spectra, the description of the measured intensities

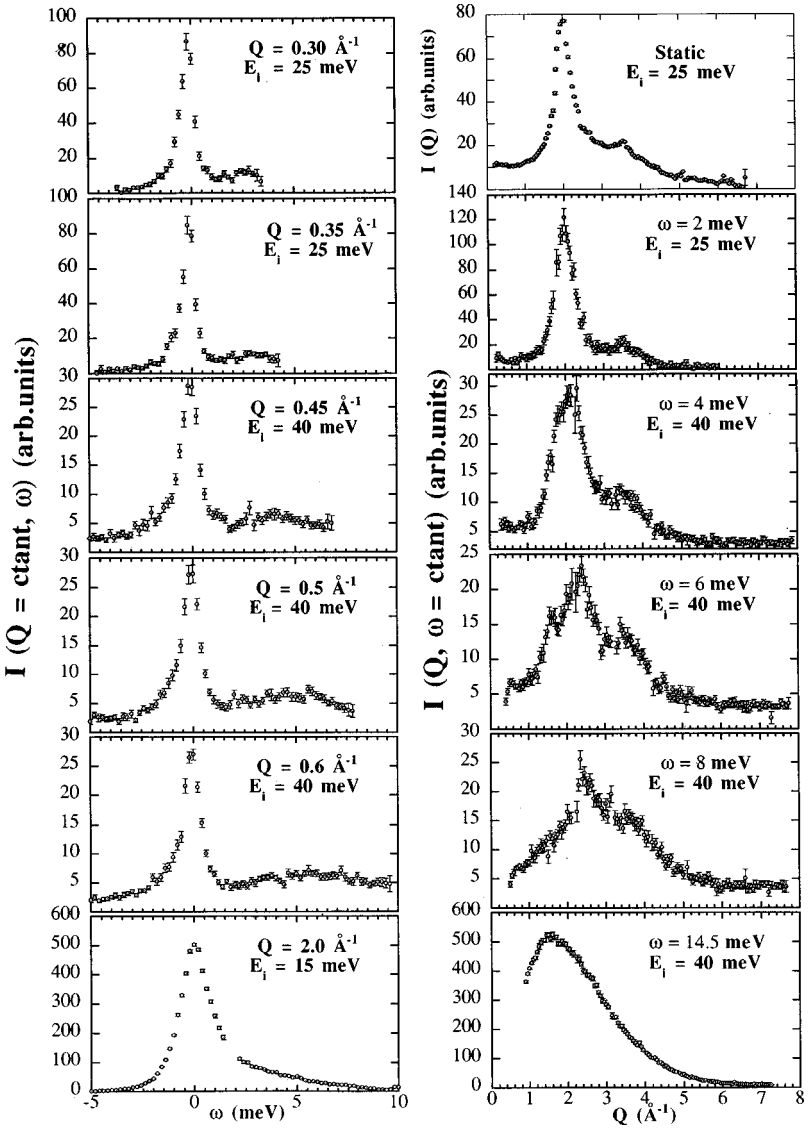

FIG. 3. The left-hand side depicts constant-Q cuts of the $Q-\omega$ surface as measured using the MARI spectrometer for Q values given as insets. The plots of the right-hand side show constant-frequency cuts for a set of values of the energy transfers given as insets. The top-right frame depicts the static structure factor as calculated from integration over accessible energy transfers of the measurement carried using an incident energy $E_i=25$ meV. It again shows that the amount o-H_2 was too low to contribute to the measured intensity.

in terms of the components contained in Eq. (4) should be considered as adequate. An assessment of the goodness of the approximation of the experimental line shapes is provided by Fig. 4, which enables a direct comparison of spectra measured on both instruments at an enlarged scale. From there, a direct comparison of the excitation line shapes as measured by both experimental techniques can be made, and shows that any possible differences are entirely attributable to differences in the technical characteristics of both spectrometers, that will possibly lead to minor differences in the fitted parameters.

The three parameters describing the Q dependence of the spectra, i.e., the strength Z_Q, the linewidth Γ_Q, and the renormalized frequency Ω_Q, are derived from fits of the referred model to the experimental intensities and are summarized in Fig. 5. Taken together, the wave-vector dependence of the three parameters clearly shows that the liquid supports a short-wavelength density oscillation which is viewed as a continuation to larger wave vectors of the excitations characteristic of an elastic fluid continuum, that is, a long-wavelength sound mode. For $Q<0.8$ Å^{-1} this mode is only weakly damped, i.e., $\omega_{co}=\Gamma_Q<\Omega_Q/\sqrt{2}$, which means that, at the lowest explored wave vectors $Q=0.25$ Å^{-1} the acoustic excitations are propagating within the liquid with mean-free paths $l=\Omega_Q/(Q\Gamma_Q)\approx 30$ Å. This is one order of magnitude larger than the equilibrium intermolecular separation $d\approx 3$ Å and is perhaps the largest found for an insulating normal liquid.

To clearly illustrate the presence of propagating short-wavelength excitations, Fig. 6 depicts the wave-vector dependence of the quotients Ω_Q/Γ_Q for both p-H_2 and o-D_2. The ω_{co} limit referred to above is crossed at about 0.75 Å^{-1} in p-H_2, but at far lower wave vectors in liquid deuterium. Collective atomic motions above such a limit become increasingly damped so that the results derived from fits to a given functional form assumed for the spectrum are somewhat dependent on the line shape of the fitting function.

IV. DISCUSSION

Simulated spectra for a set of particles interacting through the Silvera-Goldman potential are shown in Fig. 7. The plotted quantity is $\omega^2 S_{sim}(Q,\omega)$, which basically represents the longitudinal current-current correlations. This form is particularly useful since the simulated spectra show no clear peaks at finite frequencies within the explored range of wave

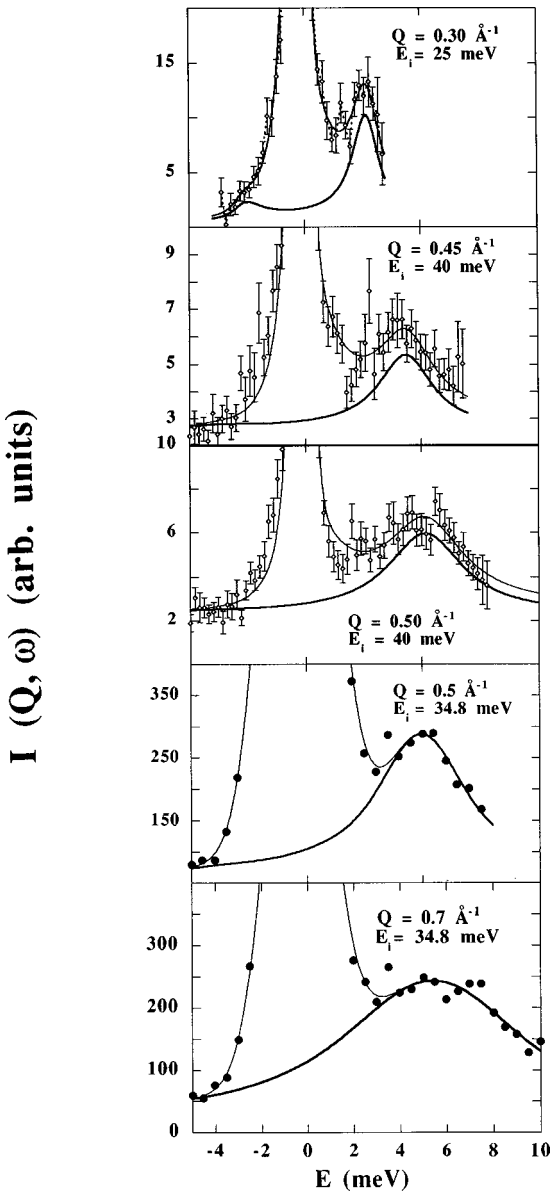

FIG. 4. A comparison of experimental and fitted spectra as measured using the MARI (upper frames) and IN8 (lower frames) spectrometers. The intensity of the inelastic wings have been largely expanded to allow comparison by the naked eye.

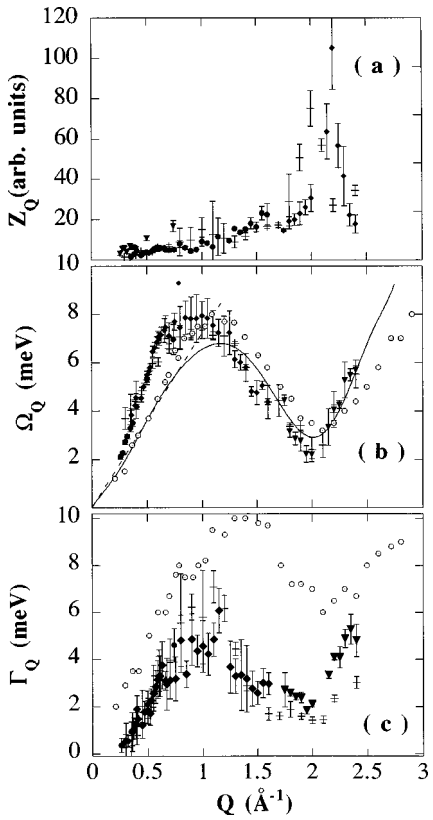

FIG. 5. Wave-vector dependence of the spectral parameters. (a) One-phonon strength Z_Q. The filled symbols (diamonds and inverted triangles) refer to MARI data using different incident energies. The crosses depict data from measurements at IN8. (b) Phonon frequency Ω_Q. The dashed line shows the hydrodynamic dispersion Ω_Q^{hyd}. The solid line show the results from a calculation using the CDM theory (Ref. 7). The filled symbols (inverted triangles and diamonds) depict data measured at MARI, the crosses show results from IN8, and the open circles with a dot show the simulation results. (c) Phonon width (damping constant) Γ_Q. The same symbols as above are used.

vectors. As seen from the figure, the spectral shapes are broad with maxima and width exhibiting a fairly strong wave-vector dependence. The maxima of those curves equal the renormalized frequency Ω_Q of the damped harmonic oscillator, although most of its value comes from the damping term Γ_Q.

The most relevant physical parameters from the simulation and the experiments are compared in Fig. 5. The most noticeable differences between experiment and simulation concerns the damping constant, which is always *much larger* in the simulation, as well as the rather different behavior at low Q of the excitation frequency. The hydrodynamic dispersion law $\Omega_Q^{hyd}=c_T Q$ is well described by the simulation and the CDM calculations for wave vectors smaller than 0.7 Å^{-1}, whereas experimental data lie above the linear law for $Q \gtrsim 0.3$ Å^{-1}. The simulation results thus portray the collective dynamics as resulting from overdamped motions down to the lowest explored wave vector $Q=0.21$ Å^{-1} or, in other words, the excitations have such a short lifetime that in no way can they be considered as propagating. Such a condition is common to most Lennard-Jones liquids close to

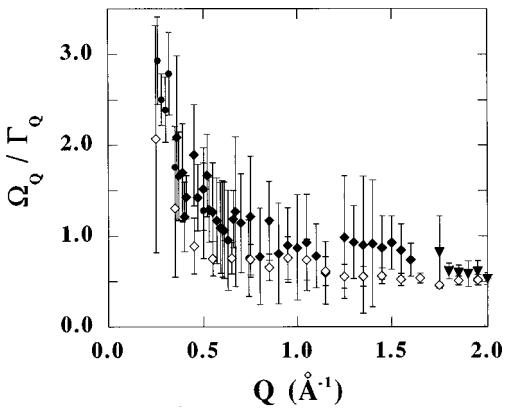

FIG. 6. Ratios between the excitation frequencies and the damping constants for liquid p-H_2 (solid symbols) and liquid o-D_2 at 20 K (Ref. 10).

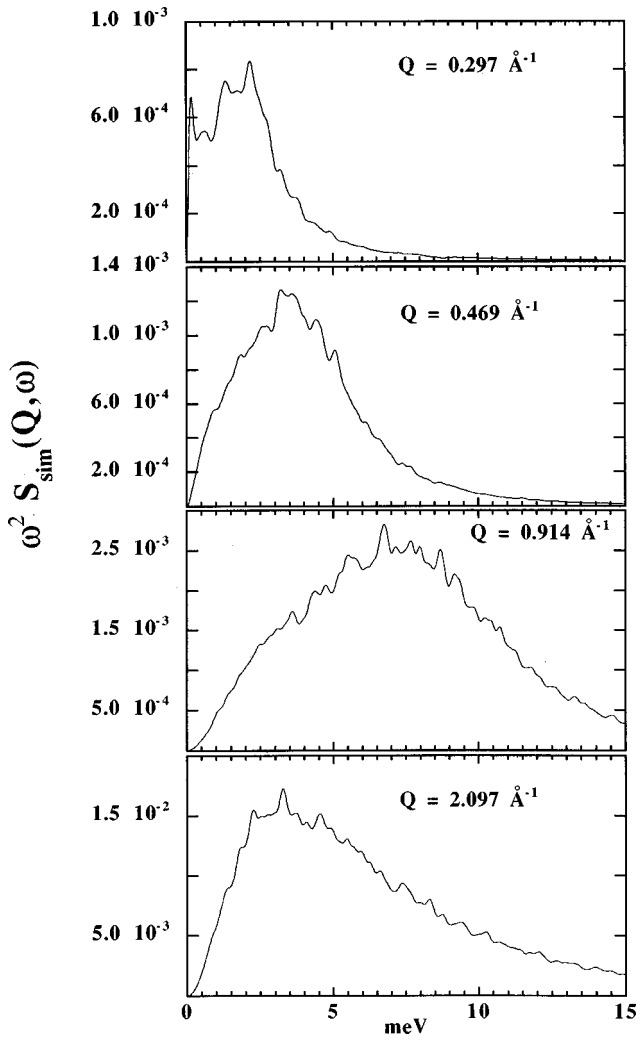

FIG. 7. Spectra resulting from the molecular-dynamics simulations are displayed as $\omega^2 S_{sim}(Q,\omega)$. The corresponding wave vectors are given as insets. The frequencies shown in Fig. 5 correspond to the maxima of spectra such as those displayed in the figure.

their triple points and arises from the relatively hard and steep interaction potentials[18] characteristic of these liquids. Since the employed potential is known to be adequate for crystalline hydrogen, the appearance in the real liquid of excitations rather well defined at least up to $Q \approx 0.8$ Å^{-1} should then be taken as an indication of the nonclassical character of the dynamics of the fluid.

The departure from hydrodynamics, usually referred to as anomalous dispersion, is a known experimental fact since work on superfluid ^{4}He,[19] liquid ^{3}He,[20] or liquid o-D_2.[10] In fact, the phenomenon is also exhibited by a weakly interacting Bose gas.[21] A convenient way to parameterize such a deviation was given by Maris,[19] and follows an equation aimed to reproduce the dispersion curve up to $Q_p/2$, viz.

$$\Omega_Q = c_T[Q + \Delta(Q)] = c_T[Q + \gamma Q^3(1 - Q^2/Q_A^2)/(1 + Q^2/Q_B^2)], \quad (5)$$

where γ controls the strength of the deviation from hydrodynamics. Such a departure, given in terms of the excitation phase velocity $c_{ph}(Q) = \Omega_Q/Q$ is thus maximal for $Q = Q_B$, whereas Q_A marks the crossover of c_{ph} to velocities

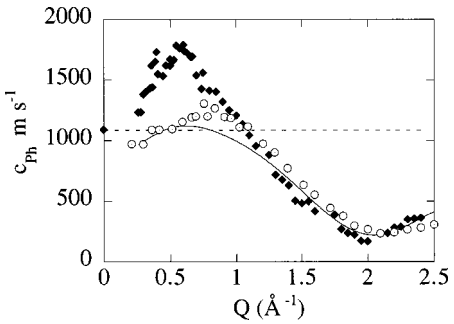

FIG. 8. Excitation phase velocities $c_{Ph}(Q) = \Omega_Q/Q$ as derived from experimental measurements (filled symbols), computer simulation (circles with a dot), and CDM calculation (solid line). The dashed line depicts the value of the isothermal sound velocity.

below c_T, which occurs at larger Q values and is shown in Fig. 8. The figure shows that the phase velocities determined from experiment approach ≈ 1800 m s^{-1} at wave vectors of $Q \approx 0.6$ Å^{-1}, whereas much weaker deviations from hydrodynamics are found in both computer simulated data and CDM results.

From a fit to experimental data for $Q \leqslant 1.2$ Å^{-1}, setting $c_T = 1096$ m s^{-1} to its macroscopic value yields $\gamma = 5.73$ Å^2, $Q_A = 1.03$, and $Q_B = 0.58$ Å^{-1}. Also, the relative deviation from hydrodynamic sound is here the largest (close to 60%) found for a simple liquid, which comes some 20 times stronger than that found for superfluid liquid ^{4}He,[17] about four times above that found for normal-phase liquid ^{4}He,[22] and about three times stronger than that observed for ^{3}He.[20]

The presence of such a large deviation from hydrodynamic sound enables the decay of phonons into two excitations, one of them having at least a lower velocity than the original phonon. In other words, an excitation with velocity well above c_T (i.e. corresponding to $Q \approx 0.5$–0.6 Å^{-1}) can decay into two excitations with velocities closer to c_T. Such a decay will yield two excitations propagating with angles $\theta_{i=1,2}$ with respect to the direction of propagation of the original phonon. A rough estimate of such angles is given by[19]

$$\theta_i \approx \sqrt{6\gamma Q_i} \simeq 40° \quad (6)$$

for a phonon with velocity close to the maximum of c_{ph} which decays into particles with velocities close to c_T and $Q_i = 0.2$ Å^{-1}. This estimate compares with $\theta \approx 10°$ found for liquid ^{4}He (Ref. 19) and thus serves to understand the microscopic origin of the far shorter mean-free paths characteristic of liquid p-H_2.

The rather weak anomalous dispersion found in the simulation data can be understood as a direct consequence of the inability of the model fluid to support finite-frequency density oscillations since all motions within the explored scales are already overdamped.

The importance of kinetic processes between excitations provides a hint to understanding some of the macroscopic thermal phenomena. In fact, it points towards the fact that the transport coefficients such as thermal conductivity and viscosity feel the effects of collisions between excitations with well defined momenta,[23] far more strongly than the liq-

uified heavier rare gases, which serves to rationalize the origin of the deviation of the transport coefficients, such as the macroscopic shear viscosity from the master curve calculated under the principle of ''corresponding states'' referred to above.[6] An estimate of the ratio between the effective times associated with the viscosity and thermal conductivity, $\tau_{eff}^{\eta}, \tau_{eff}^{\kappa}$, is given by the Prandtl number which for the thermodynamic state under consideration becomes,

$$Pr = \frac{\eta C_p}{\kappa M_H} = \frac{\tau_{eff}^{\eta}}{\tau_{eff}^{\kappa}} \approx 1.3. \tag{7}$$

It substantially deviates from the value $Pr = 0.693 \approx 2/3$ of the high-temperature gases and compares with that of the 3–4 characteristic of normal-phase liquid ^{3}He.[23,24] Such deviations are usually attributed to noticeable quantum effects which are expected for a liquid where the de Broglie wavelength $\Lambda \approx 3.1$ Å becomes comparable with the equilibrium interparticle separation. As a matter of fact, the intermolecular interaction time,[6,11] a quantity which governs the width of the depolarized Raman spectrum, was shown to deviate substantially from the alluded master curves and a rather large quantum correction was required to account for such a departure.

As shown in Fig. 5, results derived by recourse to the CDM approach are also unable to account for the anomaly just discussed. This shortcoming may be originated by a number of approximations introduced in the calculation [hypernetted chain (HNC) integral equation for the calculation of $S(Q)$ plus a somewhat unrefined form of the interaction potential which assumes a 6-12 Lennard-Jones shape].

Finally, our finding can also be understood on phenomenological grounds. In fact, the high-frequency limit of the sound absorption coefficient for a medium with high thermal conductivity is given by $\Gamma = c_T \rho C_p (c_S^2 - c_T^2)/\kappa c_S^2$ (Ref. 25) in terms of the isothermal and adiabatic sound velocities (c_T and c_S, respectively), the density (ρ), and the specific heat (C_p), and is inversely proportional to the coefficient of thermal conductivity κ. This contrasts with the standard form $\Gamma \propto (\omega^2, \kappa, \mu)$ where μ stands for the longitudinal viscosity. Consequently, sound damping at meV frequencies should be far weaker than that of a fluid with lower conductivity such as the rare-gas liquids.

V. CONCLUSIONS

In summary, unusually well defined excitations exist in liquid p-H_2 up to wave vectors of the order of 0.7 Å^{-1} showing a steep, strong anomalous dispersion. This takes place in a liquid composed by particles which are effectively spherical so that only the translational degrees of freedom are relevant. The departure from full classical behavior is also attested by the large value found for the mean-square displacement, since a large portion of it is attributable to zero-point motions. The finding of strong anomalous dispersion contrasts with phenomena observed in more complex fluids such as molten alloys or water,[26] where the dispersion is known to arise from an admixture of modes of different character. The presence of such relatively long-lived excitations thus provides a microscopic explanation for the anomalous behavior observed in its heat and momentum-transport properties.

Note added in proof. After submission of the manuscript, we became aware of a recent path-integral-molecular-dynamics calculation by Kinugawa.[27] The reported results are in at least semiquantitative agreement with our experiments.

This work was supported in part by DGICYT (Spain), Grant No. PB95-0072-C03-01.

[1] M. Ross, Rep. Prog. Phys. **48**, 1 (1985).
[2] I. F. Silvera, Rev. Mod. Phys. **52**, 393 (1980).
[3] Q. A. Korolyuk *et al.*, J. Low Temp. Phys. **111**, 515 (1998).
[4] S. W. Lovesey, *Theory of Neutron Scattering from Condensed Matter* (Oxford Science Publications, Clarendon Press, Oxford, 1984), Vol. 1, p. 214.
[5] See Ref. 4, p. 274.
[6] J. Rouch *et al.*, Physica A **88**, 347 (1977).
[7] M. L. Ristig *et al.*, in *Recent Progress in Many-Body Theories*, edited by A. J. Kallio *et al.* (Plenum, New York, 1988), Vol. 1, p. 197.
[8] K. Carneiro *et al.*, Phys. Rev. Lett. **30**, 481 (1973).
[9] F. J. Mompeán *et al.*, Phys. Rev. B **56**, 11 604 (1997).
[10] F. J. Bermejo *et al.*, Phys. Rev. B **47**, 15 097 (1993); M. Mukherjee *et al.*, Europhys. Lett. **40**, 153 (1997); M. Mukherjee *et al.*, Phys. Rev. B **57**, R11 031 (1998).
[11] P. A. Fleury and J. P. McTague, Phys. Rev. Lett. **31**, 914 (1973).
[12] W. D. Seiffert, Euratom Report No. EUR-4455-d, 1970 (unpublished); see also, J. R. Granada, V. H. Gillete, and R. E. Mayer, Physica B **156-157**, 164 (1989).
[13] J. Dawidowski, F. J. Bermejo, and J. R. Granada, Phys. Rev. B **58**, 706 (1998).
[14] W. Langel *et al.*, Phys. Rev. B **38**, 11 275 (1988).
[15] M. Nielsen, Phys. Rev. B **7**, 1626 (1973).
[16] P. E. Egelstaff, *An Introduction to the Liquid State* (Academic Press, London, 1967), p. 131.
[17] H. R. Glyde, *Excitations in Liquid and Solid Helium* (Clarendon Press, Oxford, 1994).
[18] J. W. E. Lewis and S. W. Lovesey, J. Phys. C **10**, 3221 (1977); M. Canales and J. A. Padró, Phys. Rev. E **60**, 551 (1999).
[19] H. J. Maris, Rev. Mod. Phys. **49**, 341 (1977).
[20] R. Scherm *et al.*, Phys. Rev. Lett. **59**, 217 (1987); B. Fåk *et al.*, J. Low Temp. Phys. **97**, 445 (1994).
[21] S. K. Ma, Phys. Rev. A **5**, 2632 (1972).
[22] K. H. Andersen (unpublished).
[23] H. Smith and H. H. Jensen, *Transport Phenomena* (Oxford Science Publications, Clarendon Press, Oxford, 1989), Chaps. 1 and 7.
[24] B. A. Younglove, J. Acoust. Soc. Am. **38**, 433 (1965).
[25] L. D. Landau and E. M. Lifshitz, *Fluid Mechanics* (Pergamon Press, Oxford, 1987), Chap. 8, p. 304 (Problem 3).
[26] M. Alvarez *et al.*, Phys. Rev. Lett. **80**, 2141 (1998).
[27] K. Kinugawa, Chem. Phys. Lett. **292**, 454 (1998).